Univerzita Karlova v Praze
Matematicko-fyzikální fakulta

BAKALÁŘSKÁ PRÁCE

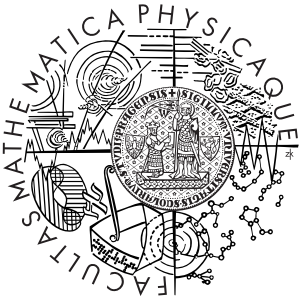

Markéta Jansová

Studium difrakčních ep interakcí na hadron-elektronovém collideru

Ústav částicové a jaderné fyziky

Vedoucí bakalářské práce: RNDr. Alice Valkárová, DrSc.
Konzultant: Mgr. Radek Žlebčík

Studijní program: Fyzika
Studijní obor: obecná fyzika

Praha 2013

Charles University in Prague
Faculty of Mathematics and Physics

BACHELOR THESIS

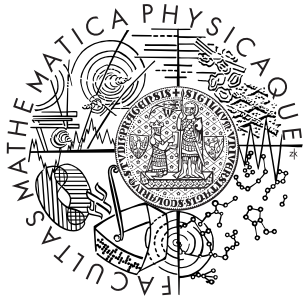

Markéta Jansová

The study of diffractive ep interactions at Hadron-Electron Collider

Institute of Particle and Nuclear Physics

Supervisor of the bachelor thesis: RNDr. Alice Valkárová, DrSc.
Consultant: Mgr. Radek Žlebčík

Study programme: Physics
Specialization: general physics

Prague 2013

Poděkování

Na tomto místě bych ráda poděkovala všem, kteří mi pomáhali a podporovali mě při vypracování této bakalářské práce. Obzvláště bych chtěla poděkovat mé vedoucí RNDr. Alici Valkárové, DrSc. za čas strávený společnými konzultacemi a za její cenné rady. Další poděkování patří Mgr. Radku Žlebčíkovi za pomoc při řešení technických i fyzikálních problémů.

Acknowledgment

Here I would like to thank all who helped me and supported me in creating of this bachelor thesis. Mainly I would like to thank my supervisor RNDr. Alice Valkárová, DrSc. for time spent consulting this thesis with me and for her valuable advice. Another thank goes to Mgr. Radek Žlebčík for his help in solving technical as well as physics problems.

Prohlašuji, že jsem tuto bakalářskou práci vypracovala samostatně a výhradně s použitím citovaných pramenů, literatury a dalších odborných zdrojů.

Beru na vědomí, že se na moji práci vztahují práva a povinnosti vyplývající ze zákona č. 121/2000 Sb., autorského zákona v platném znění, zejména skutečnost, že Univerzita Karlova v Praze má právo na uzavření licenční smlouvy o užití této práce jako školního díla podle § 60 odst. 1 autorského zákona.

V Praze dne 22.5.2013

Název práce: Studium difrakčních ep interakcí na hadron-elektronovém collideru

Autor: Markéta Jansová

Ústav: Ústav částicové a jaderné fyziky

Vedoucí bakalářské práce: RNDr. Alice Valkárová, DrSc., Ústav částicové a jaderné fyziky

Abstrakt: V CERNu je plánována výstavba *ep* collideru LHeC, který by měl doplnit fyzikální program bývalého *ep* collideru HERA a stávajícího hadronového collideru LHC. S pomocí LHeC by měly být studovány srážky elektronů o energii 60 GeV a protonů o energii 7 TeV. Práce je věnována studiu difrakčního hluboce nepružného rozptylu probíhajícího přes nabité proudy. Difrakční procesy s výměnou $W^{\pm}$ byly již zkoumány na urychlovači HERA (H1 experiment), avšak s nedostačující statistikou. Práce reprodukuje Monte Carlo předpovědi získané na H1 experimentu a jejím hlavním cílem je určení velikosti účinného průřezu difrakčního hluboce nepružného rozptylu s nabitými proudy pro budoucí LHeC projekt.

Klíčová slova: *ep* interakce, LHeC, difrakce, nabité proudy, Monte Carlo program RAPGAP

Title: The study of diffractive ep interactions at Hadron-Electron Collider

Author: Markéta Jansová

Department: Institute of Particle and Nuclear Physics

Supervisor: RNDr. Alice Valkárová, DrSc., Institute of Particle and Nuclear Physics

Abstract: A new *ep* collider LHeC is currently planned at CERN. LHeC should complement the physics program of former *ep* collider HERA and existing hadron-hadron collider LHC. In the LHeC project the collisions of electrons with energy 60 GeV and protons with energy 7 TeV should be studied. The thesis is focused on the study of diffractive charged current deep inelastic scattering interactions, which had already been investigated at HERA collider (H1 experiment), but with unsatisfying statistics. This thesis reproduce Monte Carlo predictions obtained by H1 collaboration for this process and its main goal is calculation of diffractive charged current DIS cross section for future LHeC project.

Keywords: *ep* interactions, LHeC, diffraction, charged currents, Monte Carlo program RAPGAP

Contents

Chapter 1

Introduction

Since the beginning of the 20^{th} century scattering has become an important method of studying the structure of mass. Scattering of alpha particles on a gold foil led to the formulation of the Rutherford atomic model. For further research electrons have appeared to be better choice as they interact with hadrons by electromagnetic or weak but no by strong interaction. Electron scattering has told us a lot about nuclei and nucleons' structure and until now it is an essential technique in particle physics experiments [1].

Electron proton deep inelastic scattering (DIS) provide us an insight into the parton structure of proton. DIS was explained by the parton model and the theory of quantum chromodynamics (QCD), so studying DIS offer us an information about QCD and the Standard Model validity [2]. A part of DIS events are called diffractive. Diffractive DIS events have been confusing for decades, because they could not have been described by the same theoretical framework as the rest of DIS events. For the purpose of the process description a new hypothetic particle called pomeron with quantum numbers of vacuum, not corresponding to any known real particle, had been introduced [3] [4]. Diffractive DIS provide us an unique opportunity to study the partonic structure of the pomeron.

In the following text the concept of deep inelastic scattering in ep interactions, especially the diffractive DIS, is introduced. The theoretical as well as the experimental framework is mentioned. The main focus is on diffractive charged current ep DIS, which was studied at the HERA collider (H1 experiment and ZEUS experiment) and is one of the goals of the planned LHeC project. The attempt is to reproduce the Monte Carlo prediction for the charged current diffractive DIS cross section and compare it with the data measured in the experimental conditions of the H1 experiment. Further the Monte Carlo prediction for diffractive charged current cross sections in the layout of the future electron-proton collider LHeC is given.

Chapter 2

Theoretical overview

2.1 Deep inelastic scattering

Let us consider a scattering of an electron (eventually a positron) and a proton. The scattering can be elastic or inelastic. While in elastic scattering only four-momenta of particles differ from the initial state, in inelastic scattering new particles are born.

Special case of inelastic scattering is deep inelastic scattering (DIS). Considering proton consisted of quasireal particles (partons), DIS can be described within the parton model as an interaction of point-like electron with particular parton. After a collision the struck parton decays and forms new hadrons [5]. DIS is characterized by the variable Q^2, which expresses the negative electron four-momentum transfer squared (see section 2.3). This variable is related to γ, Z^0, $W^{\pm}$ wavelength as $\lambda \sim 1/Q$. For DIS events $Q^2 \gg 1\,\mathrm{GeV}^2$.

DIS can be interpreted by the means of quantum chromodynamics (QCD). QCD is a gauge theory of the strong interaction, describing interactions between colored quarks and gluons. If scattering occurs at high Q^2, partons can be considered as nearly free particles, and DIS can be viewed in terms of a QCD perturbation theory. Perturbative QCD is suitable for the hard interactions but is not applicable for the soft ones [6].

Electrons (positrons) do not interact with protons directly but via an intermediate vector bosons (γ, Z^0, $W^{\pm}$). According to the boson's charge two kinds of DIS are distinguished, neutral and charged current DIS (see Fig. 2.1). This boson can be γ or Z^0 for neutral current (NC) interactions. In charged current (CC) DIS the exchanged boson is W^- for e^- or W^+ for e^+ interactions. Furthermore in CC DIS the incoming e^- (e^+) changes to ν_e ($\bar{\nu}_e$).

2.2 Diffractive DIS

Diffractive DIS is characteristic by substantial fraction of events with "rapidity gap" (see Fig. 2.2). The presence of rapidity gap between hadronic final state X and scattered proton (see Fig. 2.3) indicates, that the colorless object was exchanged in the interaction [8].

Roughly 10% of DIS events at HERA were of the diffractive type [8]. The name "diffractive" was derived from optics, where diffraction means reflection and decomposition of ray according to the wavelengths.

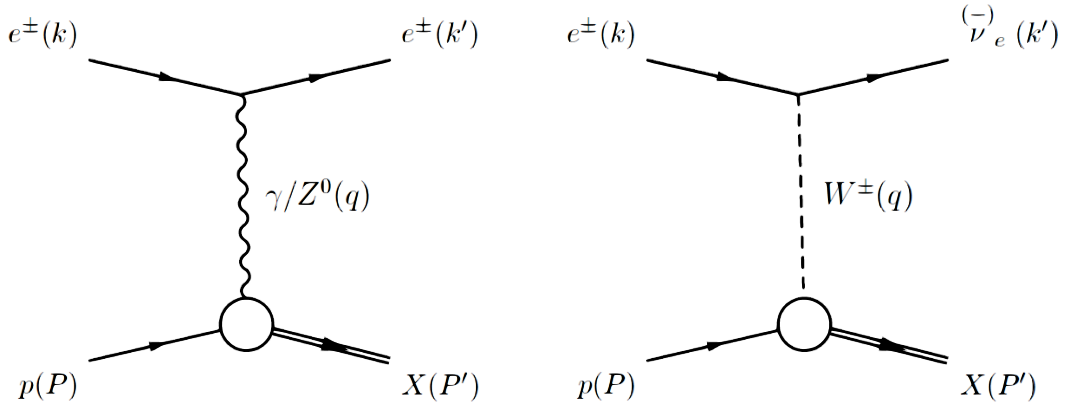

Fig. 2.1: Feynman diagrams for neutral (left) and charged (right) current DIS.

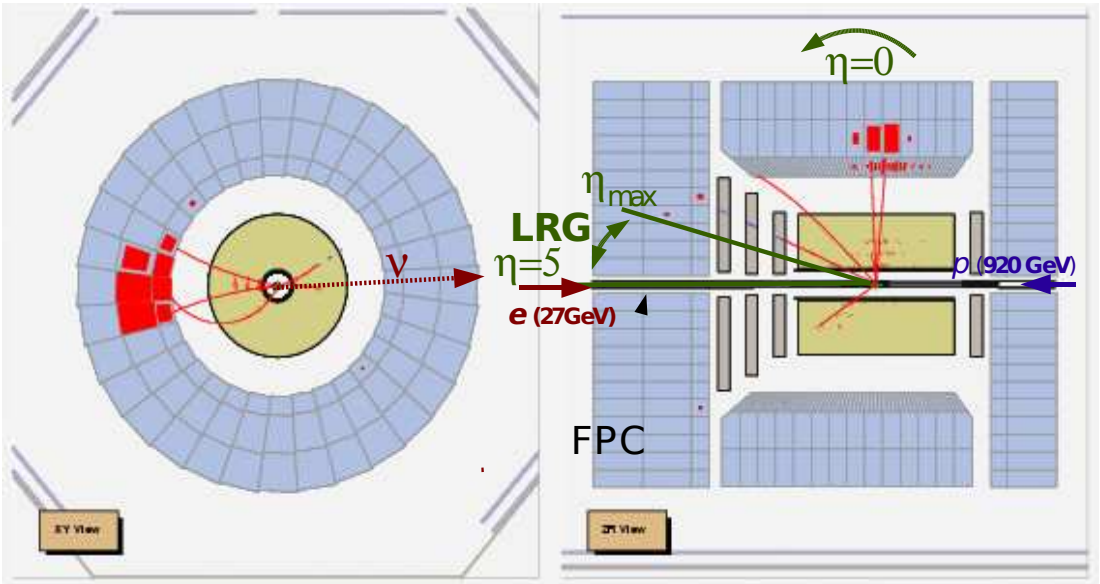

Fig. 2.2: Diffractive DIS event as seen in the detector [7].

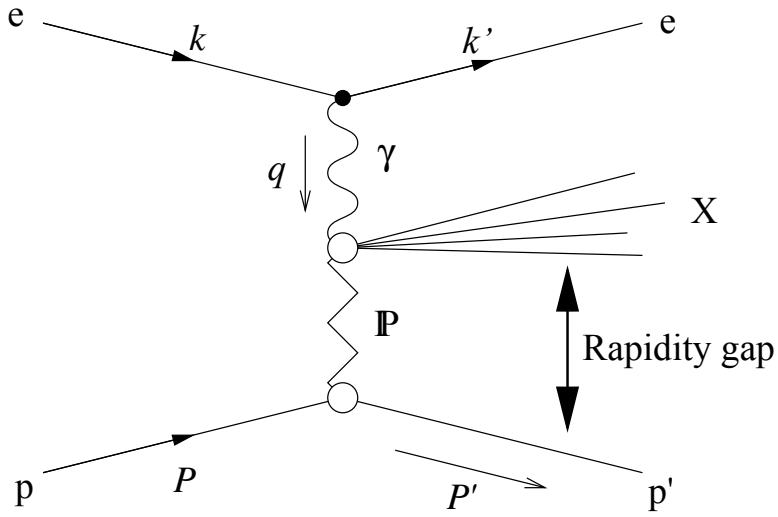

Fig. 2.3: The diffractive event significant for the rapidity gap between the system X and the scattered proton.

In *ep* diffractive DIS proton does not change its identity only its 4-momentum differs from the four-momentum of the initial state. The interaction was considered as a soft, it means, that the momentum transfer and the transverse momentum of hadronic final system X is small [9]. As mentioned before, for the soft interactions the concept of QCD perturbation theory cannot be applied. These diffractive events were explained by the colorless pomeron exchange. Later in the experimental environment of HERA collider, it was discovered, that in *ep* diffractive DIS events the hard scale is also involved. For the description of these events Ingelman and Schlein applied the concept of the "soft" pomeron to hard diffraction, assuming the partonic structure of pomeron. The hard interaction of pomeron with the virtual photon (or the massive vector boson) can be described same as the standard DIS in terms of QCD perturbation theory [10]. The small contribution to the diffractive events is also from reggeon (subleading meson) exchange.

In this theses the CC *ep* diffraction is the subject of interest. The only more detailed measurement of the charged current diffractive cross section at HERA, H1 experiment, was released by H1 collaboration in 2006 [6]. Due to unsatisfying statistics of the diffractive charged current events only a new experiment at higher energies and higher luminosity could help to understand the physics of the diffractive charged current *ep* process better.

2.3 Kinematics of diffractive DIS

Diffractive DIS neutral current

$$e^{\pm}(k)\, p(P) \rightarrow e^{\pm}(k')\, p(P')\, X \tag{2.1}$$

and charged current

$$e^{-}(k)\, p(P) \rightarrow \nu_e(k')\, p(P')X \tag{2.2}$$

$$e^{+}(k)\, p(P) \rightarrow \bar{\nu}_e(k')\, p(P')X \tag{2.3}$$

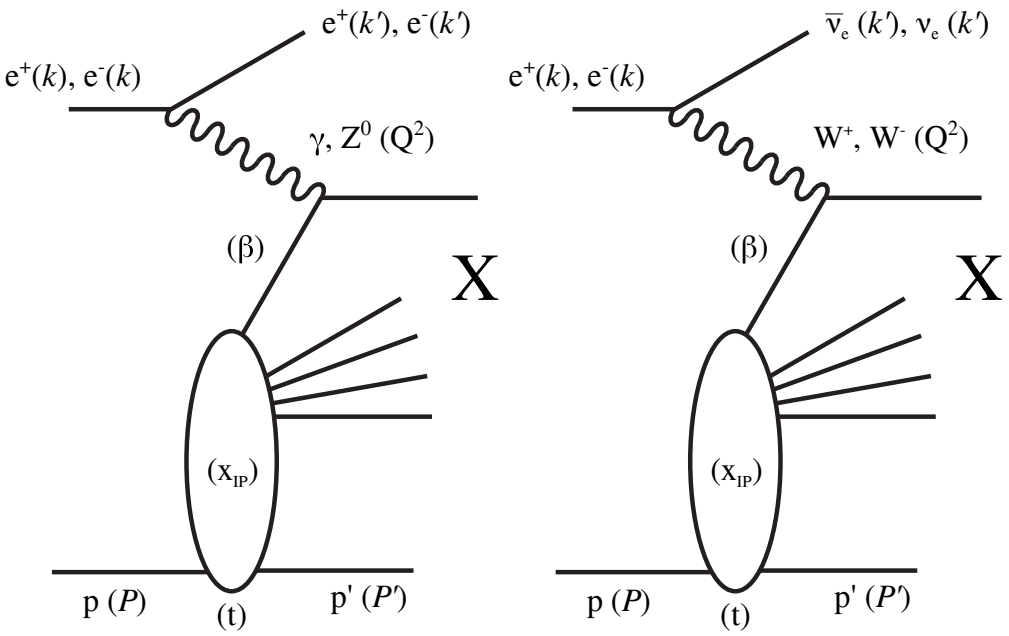

Fig. 2.4: Diagrams of diffractive neutral (left) and charged (right) current DIS.

processes are shown in Fig. 2.4. These interactions can be described by the usual DIS final state variables:

$$Q^2 = -q^2, \text{ where } q = k - k', \tag{2.4}$$

$$x = \frac{Q^2}{2Pq}, \tag{2.5}$$

$$y = \frac{Pq}{Pk}, \tag{2.6}$$

where Q^2 is the negative electron four-momentum transfer squared (boson virtuality), x is the Bjorken scaling parameter (momentum fraction of proton carried by the struck quark), y is the inelasticity of the scattering process.

For diffractive DIS extra variables were introduced:

$$x_{IP} = \frac{q(P - P')}{qP}, \tag{2.7}$$

$$\beta = \frac{Q^2}{2q(P - P')}, \tag{2.8}$$

$$t = (P - P')^2, \tag{2.9}$$

where x_{IP} is the fraction of proton's momentum carried by the diffractive exchange (pomeron), β is fractional exchanged object's momentum carried by the struck quark, $x = x_{IP}\beta$, t is the four-momentum squared carried by the diffractive exchange [6].

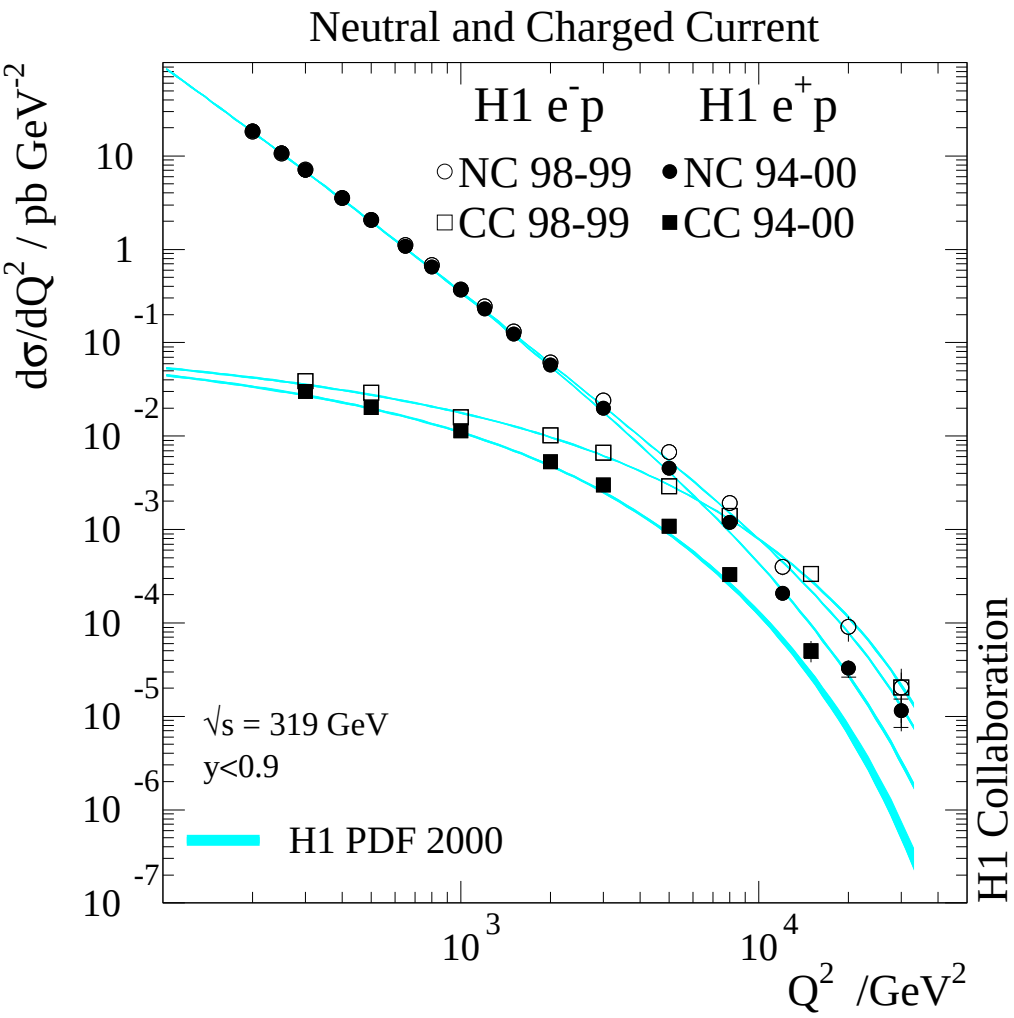

Fig. 2.5: The neutral and charged current DIS cross sections in the dependence on the Q^2 [6].

2.4 Electroweak processes

The charged current events were abundantly studied during the accelerator neutrino physics era. The neutral current interactions were predicted by S. Glashow, A. Salam and S. Weinberg. These interactions were first observed in Gargamelle bubble chamber in 1973, at CERN, Switzerland [11]. The discovery of the neutral currents proved Glashow's, Salam's and Weinberg's unification of the weak and the electromagnetic interaction, called the electroweak interaction [12]. They predicted intermediate vector bosons, which are responsible for the weak processes. Sheldon Lee Glashow, Abdus Salam and Steven Weinberg gained the Nobel Prize in Physics in 1979 "for their contributions to the theory of the unified weak and electromagnetic interaction between elementary particles, including, inter alia, the prediction of the weak neutral current" [13] [14] [15].

For the purpose of confirmation the existence of weak bosons, the high energy quark-antiquark collisions were needed. Thus the construction of new particle collider SPS (Super Proton Synchrotron) accelerating and colliding protons with antiprotons was realized. Massive Z^0 and $W^{\pm}$ bosons were first observed in 1983 [16]. The Nobel Prize in Physics 1984 was awarded to Carlo Rubbia and Simon van der Meer "for their decisive contributions to the large project, which led to the discovery of the field particles W and Z, communicators of weak interaction" [16]. The mass of Z^0 and $W^{\pm}$ bosons is explained by the Higgs mechanism predicting Higgs particle.

The electroweak theory and the theory of quantum chromodynamics build the Standard Model of particle physics [17]. The Standard model originates from a local symmetry group. S. Glashow, A. Salam and S. Weinberg assumed that all interactions are provided by gauge bosons. Thus the synthesis of strong, weak and electromagnetic interactions was established [13].

The neutral current electroweak ep process cross section differs from purely weak charged current ep process cross section in the dependence on Q^2 (see Fig. 2.5). In the low Q^2 region the exchange of γ dominates, so the cross section of neutral currents exceeds the charged current cross section by more than two orders of magnitude. For large Q^2 the γ and Z^0 contributions to NC cross section are nearly equal to $W^{\pm}$ contributions to CC cross section. In e^-p charged current interaction W^- boson is exchanged, while in e^+p it is W^+. Since each boson is sensitive to different quarks, concretely W^- boson to $u, c, t, \bar{d}, \bar{s}, \bar{b}$ and W^+ boson to $d, s, b, \bar{u}, \bar{c}, \bar{t}$ quarks, the disparity in cross sections arises from the difference between $u, c, t, \bar{d}, \bar{s}, \bar{b}$ and $d, s, b, \bar{u}, \bar{c}, \bar{t}$ quarks distributions in proton [2].

2.5 Diffractive charged currents

The only results of diffractive charged current cross section were obtained by H1 experiment [6] in 2006. There the differential cross sections were measured in dependence on x_{IP}, β and Q^2 variables and compared to Leading Order (LO) QCD Monte Carlo RAPGAP predictions (see Fig. 2.6).

In charged current DIS event at HERA, neutrino, which could not be detected in the main detector, was produced. The only signature, that the event is of charged current type, is therefore the presence of large missing transverse momentum. The CC events were identified at the trigger level using mainly the

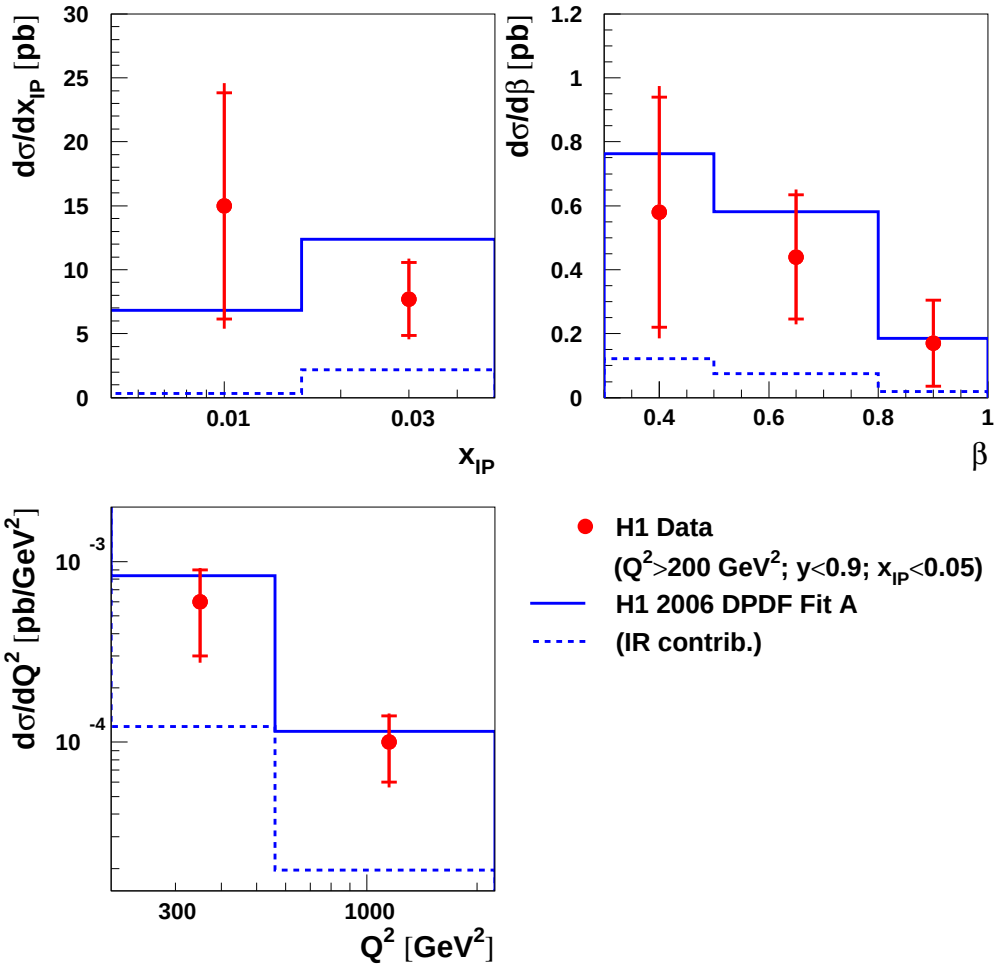

Fig. 2.6: The differential cross sections of the diffractive charged current process measured by H1 collaboration [6]. Red dots represent measured data with uncertainties. Blue lines corresponds to the MC RAPGAP predictions, dashed blue lines to the MC RAPGAP reggeon contribution only.

Liquid Argon calorimeter. The cut to transverse momentum missing was chosen to be at least 12 GeV. Since scattered proton and neutrino could not be detected, the kinematic variables were computed using hadronic final states' four-momenta. The CC differential cross sections in Fig. 2.6 have large statistical as well as systematical uncertainties. Though the measured data are in agreement with the predictions, the large uncertainties (experimental precision was about 35% of the total cross section) do not permit to make any definite conclusions [6].

Chapter 3

Electron-proton colliders

3.1 HERA

HERA was the particle accelerator situated in Hamburg's underground at DESY (Deutsches Elektronen Synchrotron) research centre, Germany (see Fig. 3.1). It was the first *ep* collider ever built. The idea to construct a "huge electron microscope for viewing the protons" was born in early 1970s and already in 1991 first collisions were held. Scientific research at HERA began in October 1992. HERA was the ring accelerator 6.3 kilometres long, 25 metres under the ground. Ten million times a second collisions were realized in two places, where H1 and ZEUS detectors were located [19].

HERA operated as "HERA I" from 1992 to 2000 and after upgrade as "HERA II" from 2003 to 2007. The energy of collided electrons (or positrons) was 27.5 GeV. The energy of protons was increased from initial 820 GeV to 920 GeV in 1998 [20]. Integrated luminosities of each period are shown in Fig. 3.2.

Measured data presented in this theses were published by the H1 collaboration [6]. At H1 experiment the structure of proton was studied. Detailed information about H1 detector is available in e.g. [21].

3.2 LHeC

Currently a new *ep* accelerator LHeC (Large Hadron Electron Collider) at CERN (Conseil Européen pour la Recherche Nucléaire) is considered. The idea is to supply the existing LHC accelerator of protons by a new electron accelerator. The proposed integral luminosity of LHeC should be about a hundred times larger than in HERA's case. The energy of proton beam would be of maximum 7 TeV, the intended energy of electron beam is 60 GeV. With these energies and luminosity much more precise data should be gained than at HERA. It is believed that this new project would deepen the understanding of the TeV scale physics, would be helpful in investigating the theory of particle physics as well as in a completing of the Standard Model and analysing the physics beyond the Standard Model.

The LHC (Large Hadron Collider) started to operate at CERN in 2008. It is the largest existing ring collider with the circumference about 27 kilometres. Protons or heavy ions are accelerated in the tunnel along which four experiments

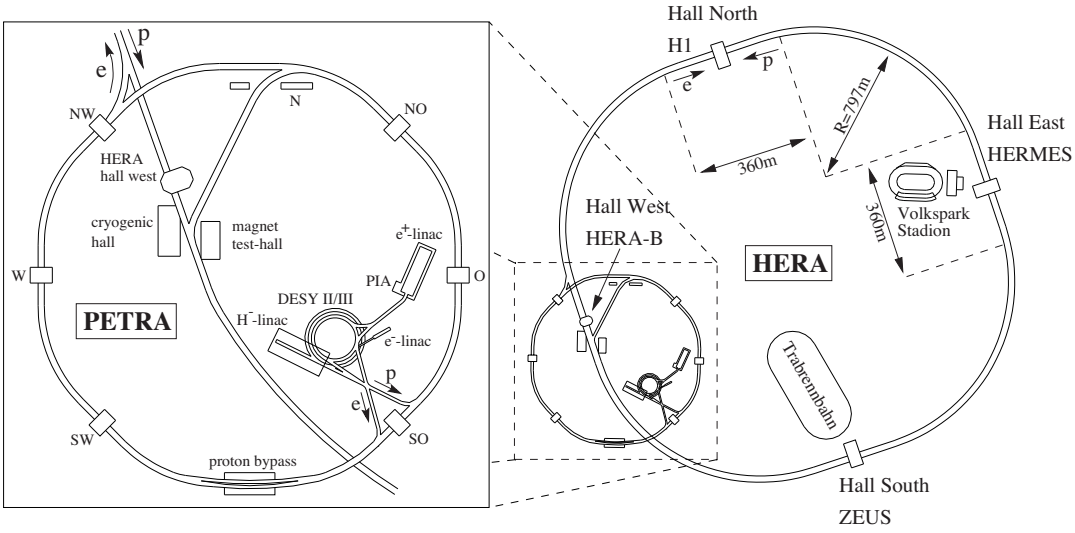

Fig. 3.1: The HERA accelerator.

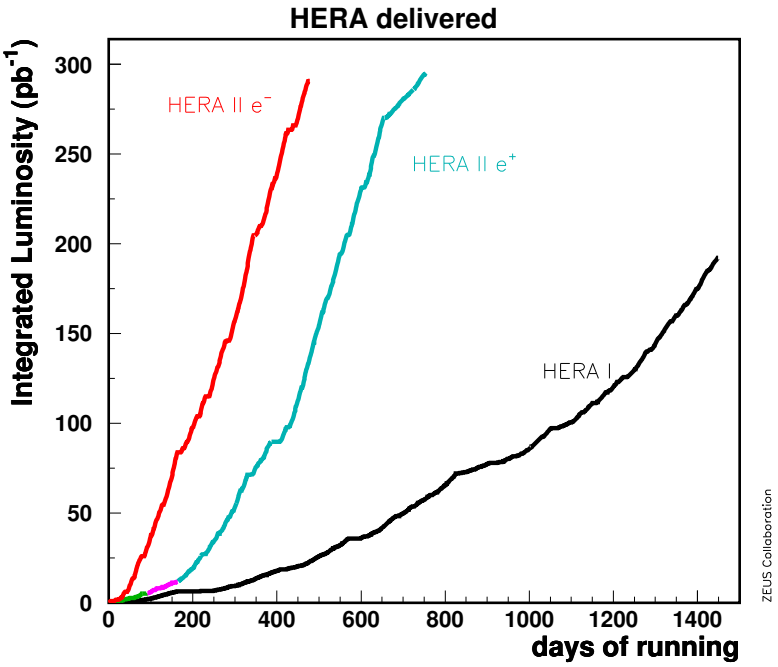

Fig. 3.2: Integrated luminosities at HERA, ZEUS experiment [18]. Luminosities at H1 are similar.

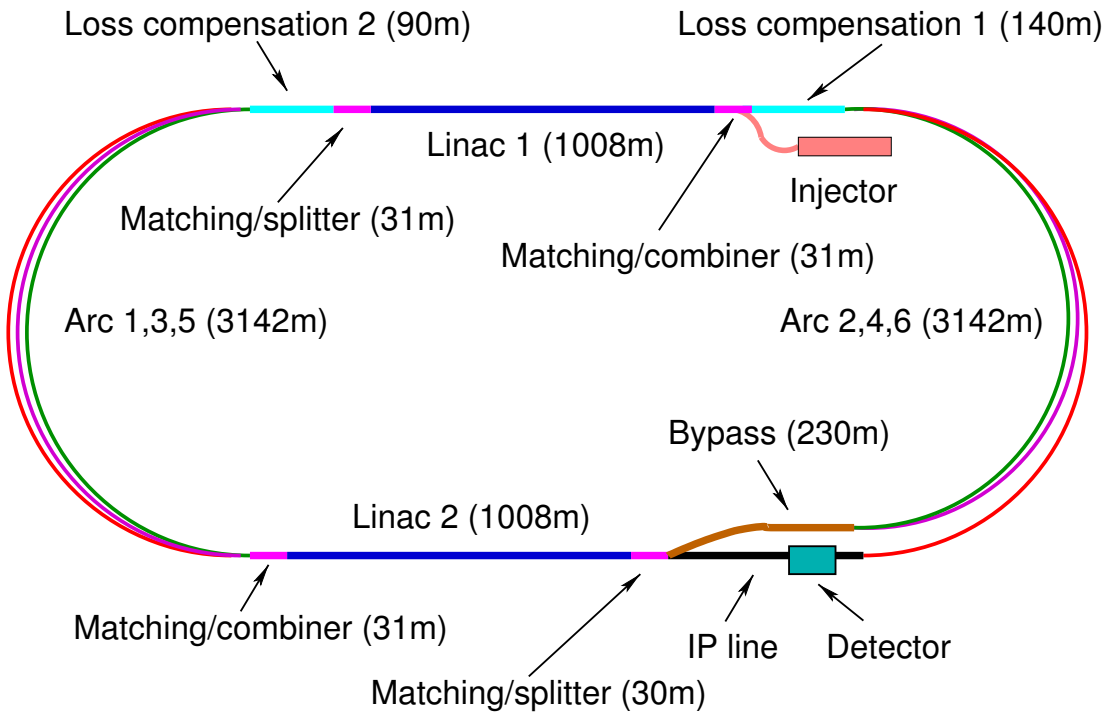

Fig. 3.3: The LHeC linac collider configuration [22].

are situated. The LHC's purpose was to test the Standard Model, reject or confirm the Higgs mechanism connected with the Higgs particle designed to explain the origin of mass, study the dark matter, examine the quark gluon plasma and generally provide the environment to the further research in the particle physics. More information can be found in [23] [24] [25] [26] [27].

The LHeC should complement the LHC's program and answer some open questions. An important task is to study predicted leptoquarks, the states between quarks and leptons. The LHeC would provide opportunity to measure Higgs boson's properties in a detail. The research would focus on the purpose of gluon, mapping the gluon field, studying the deeply virtual Compton scattering and much more [28].

Significant task is to test the validity and to develop the knowledge of QCD, which is one of the basic theories of the Standard Model. Precious measurement of diffractive DIS is one of the probes. Besides this, considerable goals of diffractive DIS experiments are to test the approach to diffractive DIS (based on parton distribution functions) and its applicability to predict hadron-hadron scattering process. Another aim is the investigation of the partonic structure of the pomeron [29].

The LHeC study group proposes that the construction of the LHeC should be finished in next ten years. The anticipated integrated luminosity is about order of $100\,\mathrm{fb}^{-1}$. The considered options for LHeC was the ring-ring and linac-ring collider configurations. The favorable configuration is the linac-ring (see Fig. 3.3) [22].

The detector is intended to take data in a high acceptance mode, covering polar angles $1^\circ < \Theta < 179^\circ$ (the angle is measured in respect to the incoming proton), at a reduced luminosity and in a reduced acceptance mode at a high

luminosity for angles $8^\circ < \Theta < 172^\circ$ [28]. These modes are only considerations and their unification is probable.

In the case of charged current DIS the nascent neutrino cannot be detected. The diffractive events can be selected either by large rapidity gap (LRG) method [8] or by direct measurement of forward proton. In the LRG case no hadronic activity in the forward detector region is required, which ensures that the majority of selected events is diffractive. The diffractive proton leaves the interaction undetected, so the whole event kinematics must be extracted from the hadronic final state. Detection of the proton can provide more precise values of x_{IP} and in contrast to LRG method t variable can be measured. For detailed detector considerations see [28].

Chapter 4

Monte Carlo models

4.1 Monte Carlo programs

Monte Carlo (MC) programs are used to generate particle collisions according to certain physics model. For specific initial configurations of beam particles with particular four-momenta, large number of final states are generated. The frequency of certain final state arrangement is determined by its cross section. Interactions are calculated on the parton level but only hadrons, not partons, can be observed, so the phenomenological model of hadronisation had to be added [30].

Monte Carlo models are also used for determination of detector acceptance and resolution corrections. In the analysis of detector's data the MC generated events, which were passed through the simulated detector, are used for unfolding of the data to the hadron level. In the case of the LHeC the detector configuration is not yet established, so the simulation of real events in the detector cannot be provided.

4.2 Monte Carlo generator RAPGAP

The provided analysis is based on the MC generator RAPGAP. RAPGAP is LO MC model, which was created to describe deep inelastic scattering, non - diffraction, diffraction and π exchange as well as resolved virtual processes [31].

The events in this thesis were generated by the special version of RAPGAP 3.1 designed for modeling diffractive *ep* scattering. In RAPGAP several models for diffraction are available. The model chosen by myself as well as by H1 collabaration is mix of pomeron and subleading reggeon exchange introduced as "resolved pomeron model" by Ingelman and Schlein [32].

For simulation of the diffractive events RAPGAP uses the diffractive parton distribution functions DPDFs (describing "diffractive structure of proton") gained from QCD fits of measurements the diffractive interactions. H1 2006 DPDF Fit A and H1 2006 DPDF Fit B were extracted from diffractive neutral current inclusive measurements done by H1 collaboration [6]. Later it was found, that DPDF Fit B is more reliable to describe diffractive DIS dijet production than Fit A.

The implemented hard subprocesses in RAPGAP 3.1 describing diffractive

charged current DIS events are [31]:

$$eq \rightarrow \nu q', \tag{4.1}$$

$$eg \rightarrow \nu q' \bar{q}, \tag{4.2}$$

$$eg \rightarrow \nu s \bar{c}, \tag{4.3}$$

$$eq \rightarrow \nu q' g, \tag{4.4}$$

where e denotes electron, ν neutrino, q ($\bar{q}$) denotes u, d, s ($\bar{u}, \bar{d}, \bar{s}$) quarks, g gluon and c charm quark.

Chapter 5

Reconstruction formulae of the kinematic variables

The fundamental feature of charged current events is seeming "violation" of the transverse momentum conservation law. Weakly interacting neutrino escapes undetected and causes missing transverse momentum p_{Tmiss}. Supposing that scattered proton changes its direction only a little, proton's transverse momentum can be neglected. Therefore transverse momentum of neutrino p_{Tmiss} is equal to transverse momentum of hadronic system (without diffractive proton). The selection of CC events is based on this striking observation.

For the purpose of computing the kinematic variables, four-momentum of hadronic system have to be reconstructed. Then angle Θ_ν and energy E_ν of neutrino can be expressed as:

$$\Theta_\nu = 2 \arctan \frac{\frac{p_{Tmiss}}{\tan \Theta_h} - E_h + 2E_e}{p_{Tmiss}}, \tag{5.1}$$

$$E_\nu = \frac{\frac{p_{Tmiss}}{\tan \Theta_h} - E_h + 2E_e}{2} + \frac{p_{Tmiss}^2}{2\frac{p_{Tmiss}}{\tan \Theta_h} - 2E_h + 4E_e}, \tag{5.2}$$

where Θ_h is angle of hadronic system in respect to incoming proton, E_h is energy and p_{Tmiss} is transverse momentum of hadronic system. E_e is beam energy of electron.

Energy $E_{p'}$ of outgoing proton is:

$$E_{p'} = E_p + E_e - E_\nu - E_h, \tag{5.3}$$

where E_p is energy of incoming proton.

The basic kinematic variables stated in (2.3) can be calculated as:

$$Q^2 = 4E_e E_\nu \cos^2 \frac{\Theta_\nu}{2}, \tag{5.4}$$

$$y = 1 - E_\nu \frac{1 - \cos \Theta_\nu}{2E_e}, \tag{5.5}$$

$$x_{IP} = 1 - \frac{E_{p'}}{E_p}, \tag{5.6}$$

$$t = -4E_p E_{p'} \sin^2 \frac{\Theta_{p'}}{2}, \tag{5.7}$$

$$\beta = \frac{Q^2}{4E_e E_p y x_{IP}}, \tag{5.8}$$

where Q^2 is the negative electron four-momentum transfer squared, y is the inelasticity of the scattering process, x_{IP} is the fraction of proton's momentum carried by the diffractive exchange, t is the four-momentum squared carried by the diffractive exchange, β is fractional exchanged object's momentum carried by the struck quark [6]. The mass of proton and electron was neglected.

Chapter 6

Results - Diffractive CC cross section at HERA

6.1 The H1 measurement and prediction of CC cross section

The only measurement of diffractive charged current cross section was published by H1 collaboration in 2006 [6]. The experiment studied collisions of positrons with energy 27.5 GeV and protons with energy 920 GeV. The analysis cuts $Q^2 > 200\,\mathrm{GeV}^2$, $y < 0.9$ reject events with small missing transverse momentum (detector-level selection requires $p_{Tmiss} > 12\,\mathrm{GeV}$) and ensure reasonable containment of the hadronic system in the central detector.

The total diffractive charged current cross section measured by H1 collaboration in the kinematic region $Q^2 > 200\,\mathrm{GeV}^2$, $y < 0.9$, $|t| < 1\,\mathrm{GeV}^2$ and $x_{IP} < 0.05$ is

$$\sigma^{H1}_{DCC} = 390 \pm 120\,(\mathrm{stat.}) \pm 70\,(\mathrm{syst})\,\mathrm{fb}. \tag{6.1}$$

In the Fig. 2.6 the measured diffractive charged current data in dependence on x_{IP}, β and Q^2 are shown [6]. The experimental results are compared with the MC RAPGAP using 2006 DPDF Fit A (see sect. 4.2). From Fig. 2.6 is seen that the reggeon contribution represents about 15% of the differential cross section for $x_{IP} > 0.015$ and for lower x_{IP} is negligible.

Only 10 events satisfying the kinematic region $Q^2 > 200\,\mathrm{GeV}^2$, $y < 0.9$, $|t| < 1\,\mathrm{GeV}^2$ and $x_{IP} < 0.05$ were found by H1 experiment. The measured data are in agreement with the MC predictions, but due to small statistics any definite conclusions cannot be made [6].

6.2 Reproduced prediction for the H1 CC cross section

My first task was to reproduce the Monte Carlo prediction obtained by H1 collaboration [6] in the identical kinematic region. The further development of Monte Carlo model RAPGAP has continued since the results [6] were published. Older versions of RAPGAP and especially used steering files are not available now.

Results obtained by myself are based on events generated by RAPGAP 3.1, using pomeron and reggeon exchange model, DPDF Fit A and considering processes (4.1 - 4.4). Applying integrated luminosity $61.6\,\mathrm{pb}^{-1}$ [6], the number of events surviving the cuts is ~ 20. By comparison with 10 events measured by H1 collaboration, it can be deduced, that the events selection efficiency was about 50%. The total MC diffractive charged current cross section is

$$\sigma^{H1}_{MC,DCC} = 340\,\mathrm{fb}. \tag{6.2}$$

The total MC cross section obtained by H1 collaboration is $\sim 360\,\mathrm{fb}$.

The diffractive CC differential cross sections are shown in Fig. 6.1. In the figure measured (red points), RAPGAP predicted (blue solid lines) differential cross sections and reggeon contribution (blue dashed lines) from [6] can be seen. Furthermore there are the RAPGAP predictions for differential cross sections (pinkish solid line) and reggeon contributions (pinkish dashed lines) done by myself. The MC RAPGAP differential cross sections given in [6] and my RAPGAP differential cross sections are within negligible statistical errors, because of the finite MC sample, not fully identical. This is mainly due to different reggeon contribution in both cases. As stated before, it is impossible to reproduce exactly the RAPGAP setup used in [6]. Keeping this in mind, the conclusion is, that the agreement of both predictions is quite sufficient and this version of RAPGAP can be also used for LHeC predictions.

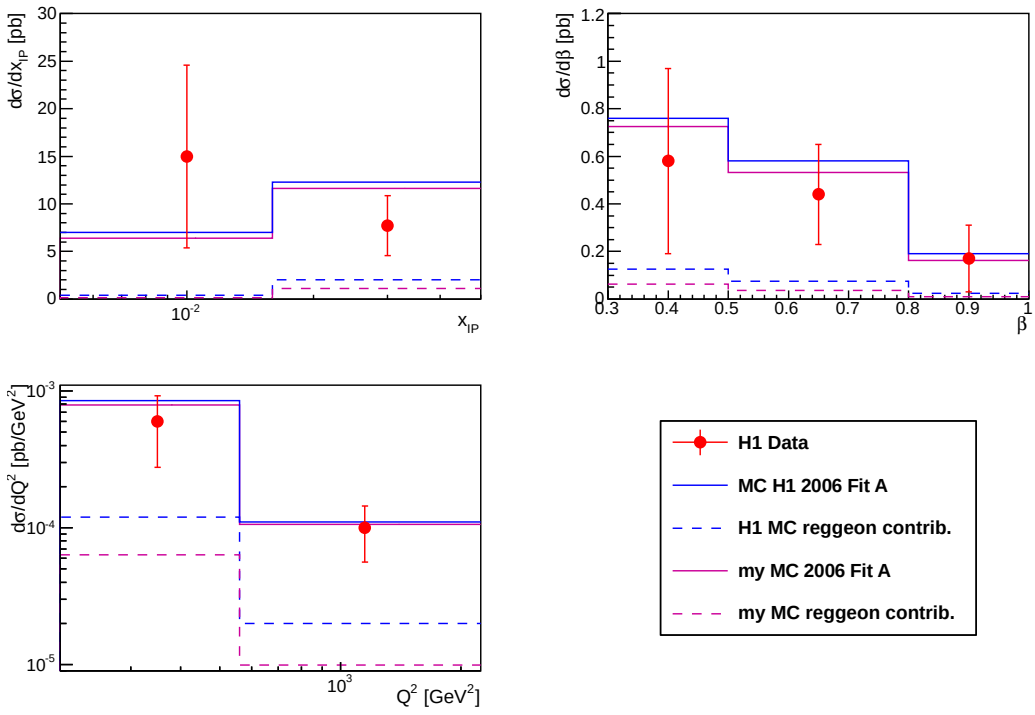

Fig. 6.1: The measured and the MC RAPGAP differential diffractive charged current cross sections in x_{IP}, β and Q^2, in the kinematic region $Q^2 > 200\,\mathrm{GeV}^2$, $y < 0.9$, $|t| < 1\,\mathrm{GeV}^2$ and $x_{IP} < 0.05$. The red points (with error bars) are data measured by H1 collaboration and the blue solid lines their predictions [6]. The H1 reggeon contributions were drawn in blue dashed lines. My predictions are shown in pinkish solid lines and the reggeon contributions in pinkish dashed lines. The MC statistical errors are negligible.

Chapter 7

Results - Diffractive CC cross section at LHeC

7.1 The selection of the MC generated events

The main task was to predict diffractive charged current cross section in the experimental conditions of LHeC. In the LHeC design report [28] is the stated electron's energy 60 GeV, proton's energy 7 TeV, integrated luminosity of order 100 fb^{-1}. The concrete detector acceptance is not known. The considerations for the detector acceptance according to the design report [28] are $1^\circ < \Theta < 179^\circ$ eventually $8^\circ < \Theta < 172^\circ$, Θ is the angle of outgoing particles measured in respect to the direction of incoming proton.

Detector cuts for angle Θ_h and missing transverse momentum p_{Tmiss} used in this thesis are following:

$$8^\circ < \Theta_h < 172^\circ, \; p_{Tmiss} > 20\,\text{GeV}, \tag{7.1}$$

where the cut for p_{Tmiss} restricts background stemming from the diffractive ep photoproduction. The fraction of background with this p_{Tmiss} cut is unfortunately not known.

First suggested kinematic region was:

$$Q^2 > 200\,\text{GeV}^2, \; 0.005 < x_{IP} < 0.012, \; |t| < 13\,\text{GeV}^2, \tag{7.2}$$

where the cuts for x_{IP} and $|t|$ were taken from the design report [28] (see Fig. 7.1).

Further it is supposed, that the outgoing proton will be measured in the forward proton spectrometers, but all variables (except t) could be calculated only from the hadronic final state four-vector, concretely from the energy E_h, the transverse momentum p_{Tmiss} and the angle Θ_h (in respect to the incoming proton) of the whole hadronic system (see chap. 5). The kinematic variables were calculated using equations (5.4 - 5.8). The chosen angle acceptance and the minimum of missing transverse momentum for hadronic final state in this study is given in (7.1). Analyzed events were generated by the Monte Carlo generator RAPGAP using 2006 DPDF Fit B (4.2) considering processes (4.1 - 4.4).

First the kinematic region, in which the majority of measurable events lies, had to be determined. For this purpose the important correlation plots of variables Q^2, Θ_h, p_{Tmiss} and y are plotted in the Fig. 7.2 using cuts (7.2). It is evident,

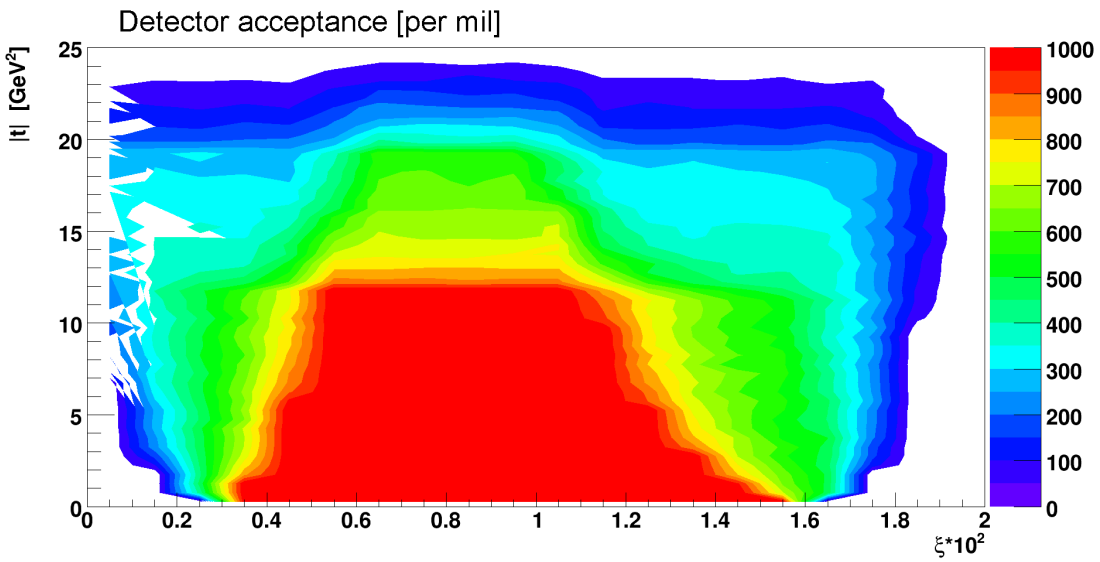

Fig. 7.1: The acceptance for the proton detector in the dependence on the four-momentum transfer squared $|t|$ and the momentum loss ξ (ξ is an alternative symbol for x_{IP}) [28].

that events with small Q^2 are dominant. The angle as well as the transverse momentum of the hadronic state has tendency to grow with increasing Q^2. This observation led to proposal of larger cut for Q^2 in order to suppress events with small p_{Tmiss} and Θ_h. Also there is an obvious tendency to growth of the hadronic final state's angle with increasing y.

Another view on the kinematic region is shown in the Fig 7.3. In the figure the detector selection efficiency A is visualised. It is defined as the ratio of events which were selected by cuts (7.1) and (7.2) to all events in the studied kinematic region (cutted only by (7.2)). It depicts percentage of events, which can be measured by detector and do not lay in the part of phase space with large background contamination. From the Fig. 7.3 can be seen, that for events with large y the acceptance is much smaller than 1. Consequently the cut for large y was introduced, because systems with large y are often scattered backwards and have small p_{Tmiss}.

For the further examination of the kinematic region (7.2) Fig. 7.4 was plotted. In the Fig. 7.4 (left) are the differential distributions of number of hadrons per event going to Θ angle (differential particle multiplicity). The areas of distributions in 7.4 (left) are normalized to the mean number of hadrons produced in the event. From the figure is obvious, that hadrons have tendency to deposit their energy in small Θ angle. The large number of hadrons going to small angles was reduced by the cut for small y. At low values of y the hadronic system is scattered in the forward direction and substantial part of the hadronic system cannot be detected. In the Fig. 7.4 (right) are the histograms of the ratio of energy lost E_{lost} caused by undetectable hadrons to total energy E of the event. The mean energy loss is about 38%. The surfaces of distributions in the Fig. 7.4 (right) are normalized to 1. For both figures the pinkish solid lines corresponds to events selected by (7.1) and the black dotted were cutted by both (7.1) and (7.2).

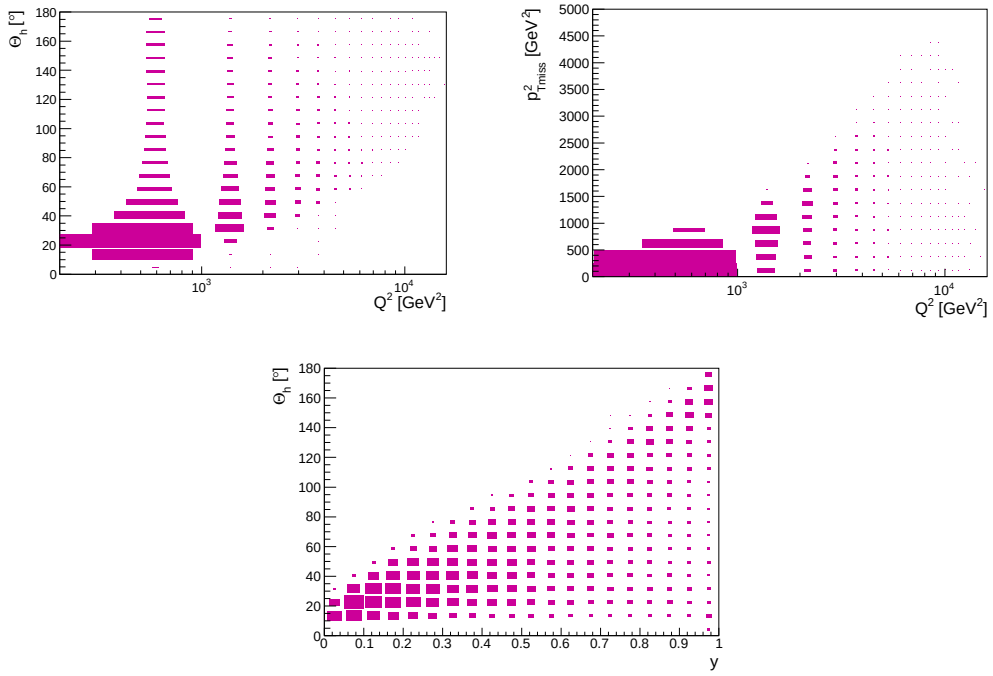

Fig. 7.2: Two dimensional histograms. **Left top** - the correlation of the hadronic state angle Θ_h and Q^2. **Right top** - the correlation of the hadronic state transverse momentum squared p^2_{Tmiss} and Q^2. **Bottom** - the correlation of the hadronic state angle Θ_h and y. The kinematic region is given in (7.2).

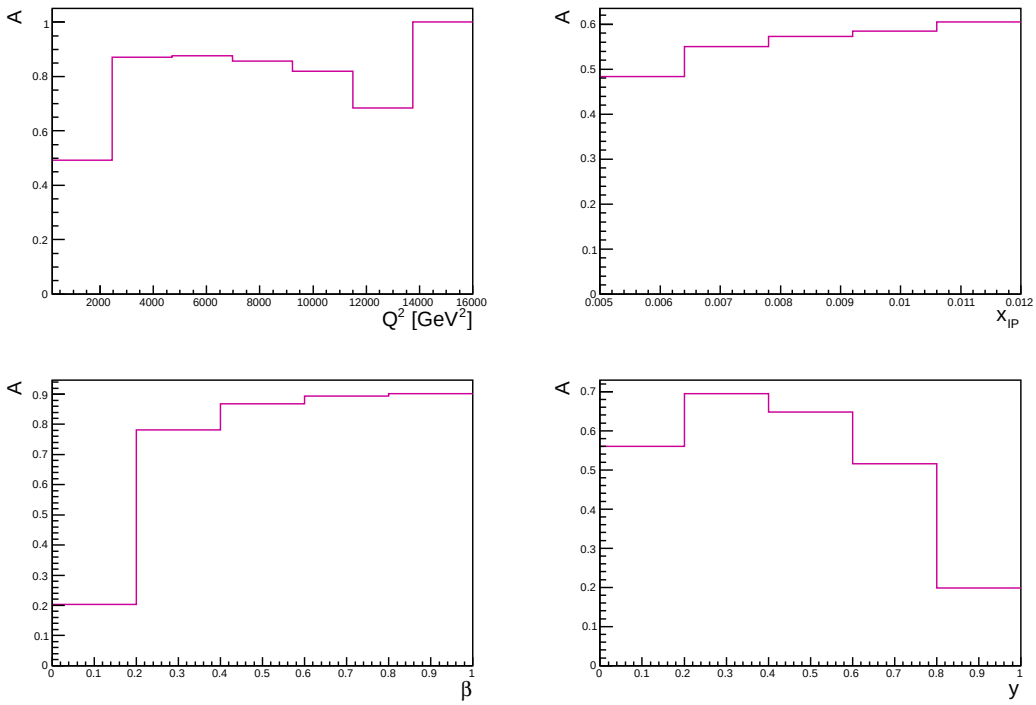

Fig. 7.3: The events selection efficiency A in the dependence on Q^2, x_{IP} β and y. $A \times 100$ is the percentage of events which can be measured by the detector. The kinematic region is given in (7.2).

For the better notion the differential cross sections of the hadronic state angle and transverse momentum in the kinematic region (7.2) are demonstrated in one dimensional histograms (see Fig. 7.5). It is clearly seen, that the kinematic region have to be changed to avoid the presence of events with small Θ_h and p_{Tmiss}.

Then the kinematic region was improved in respect to the detection constraints:

$$Q^2 > 700\,\mathrm{GeV}^2,\ 0.2 < y < 0.9,\ 0.005 < x_{IP} < 0.012,\ |t| < 13\,\mathrm{GeV}^2. \qquad (7.3)$$

After all considerations above, the kinematic region was changed to (7.3) and all figures were redrawn. In the Fig. 7.6 can be seen that by the suitable choice of the kinematic region, the events fulfill detection constraints better than in the Fig. 7.2. Also the acceptance was improved (see Fig. 7.7). From the Fig. 7.8 (left) is seen, that small difference between the two distributions was achieved, and therefore almost all events are measurable. The mean energy loss (see Fig. 7.8) (right) was diminished to 34%. In the Fig. 7.9 is shown, that the majority of events in this kinematic region can be detected in central part of detector and only low fraction of events is undetectable. From the figure it is obvious that the events with small transverse momentum were reduced too.

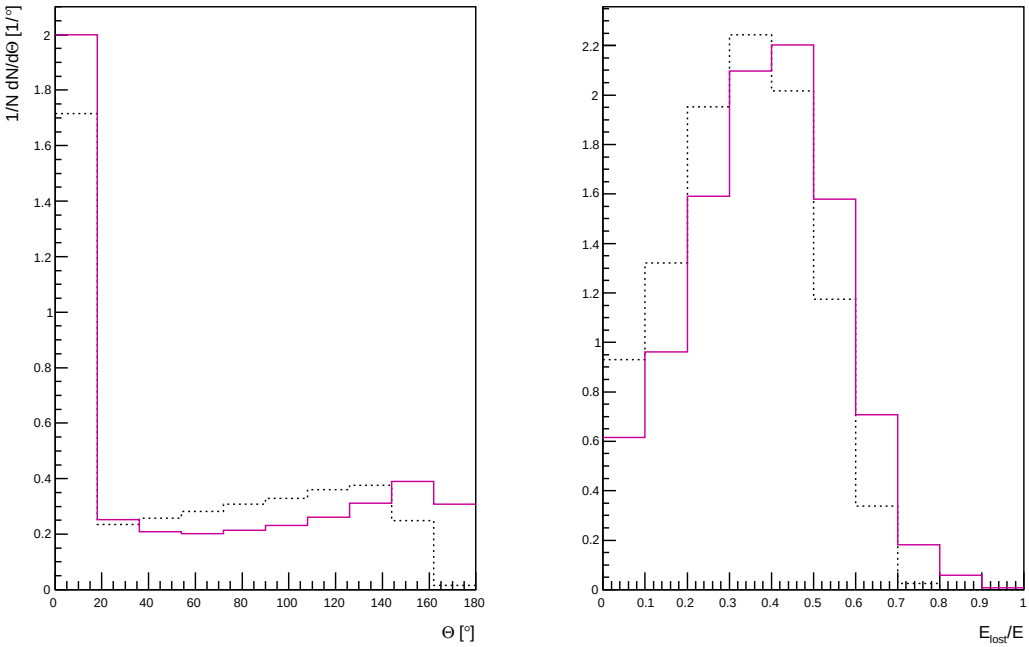

Fig. 7.4: **Left figure:** The differential distribution of number of hadrons per event going to Θ angle. The histogram is normalized to the mean number of hadrons produced in event. **Right figure:** The histogram of the ratio of lost energy E_{lost} (caused by undetectable hadrons) to total hadronic final state energy E. The histogram is normalized to 1. For both figures the pinkish solid lines are the histograms of events, which satisfy the (7.2) cuts, the dotted black lines are the histograms of events, which were cutted by both (7.2) and (7.1) cuts.

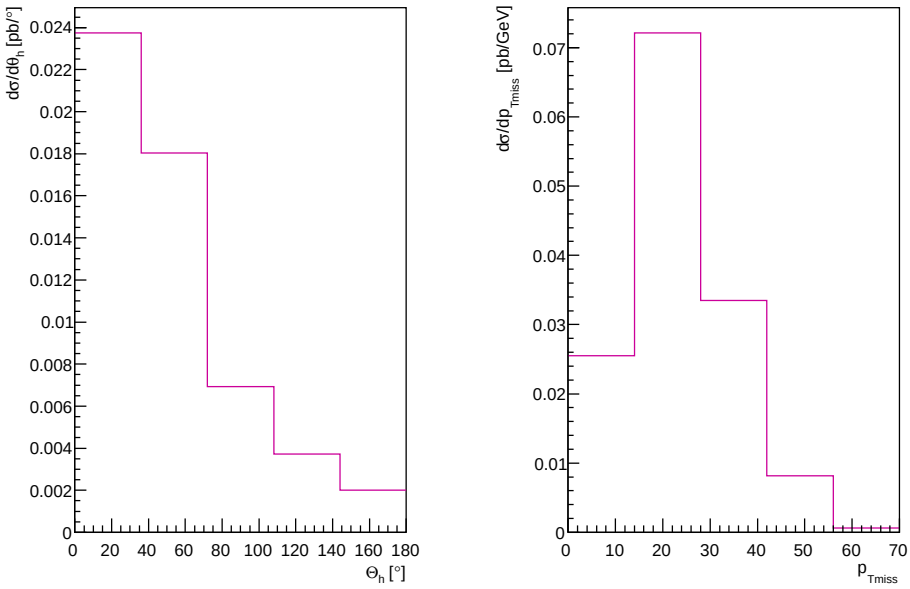

Fig. 7.5: The differential cross sections of the hadronic state angle Θ_h and transverse momentum p_{Tmiss}. The kinematic region is given in (7.2).

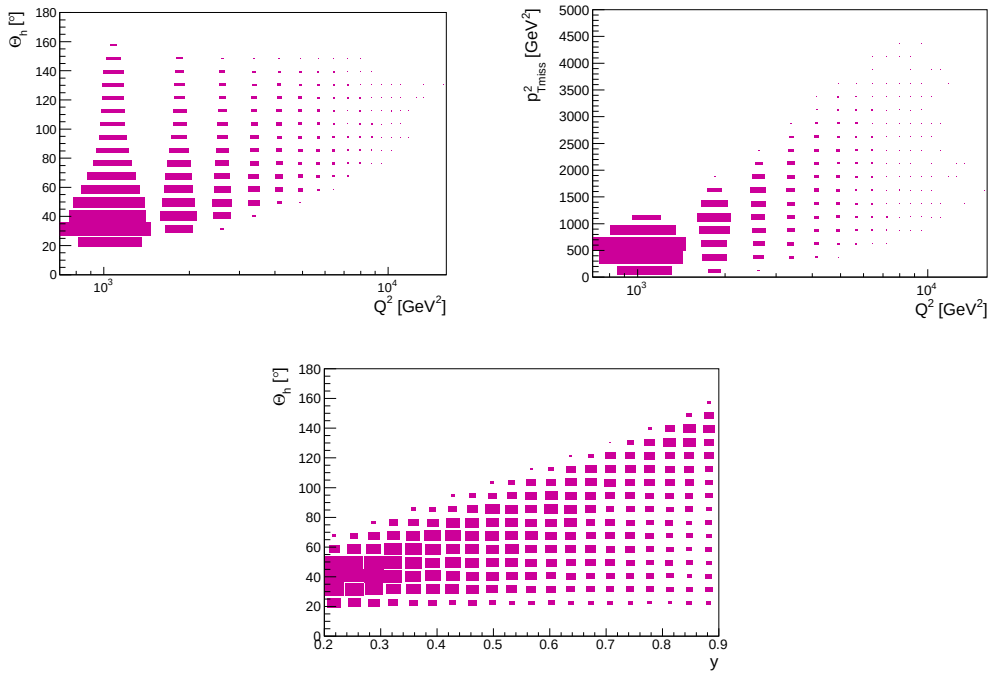

Fig. 7.6: Two dimensional histograms. **Left top** - the correlation of the hadronic state angle Θ_h and Q^2. **Right top** - the correlation of the hadronic state transverse momentum squared p^2_{Tmiss} and Q^2. **Bottom** - the correlation of the hadronic state angle Θ_h and y. The kinematic region is given in (7.3).

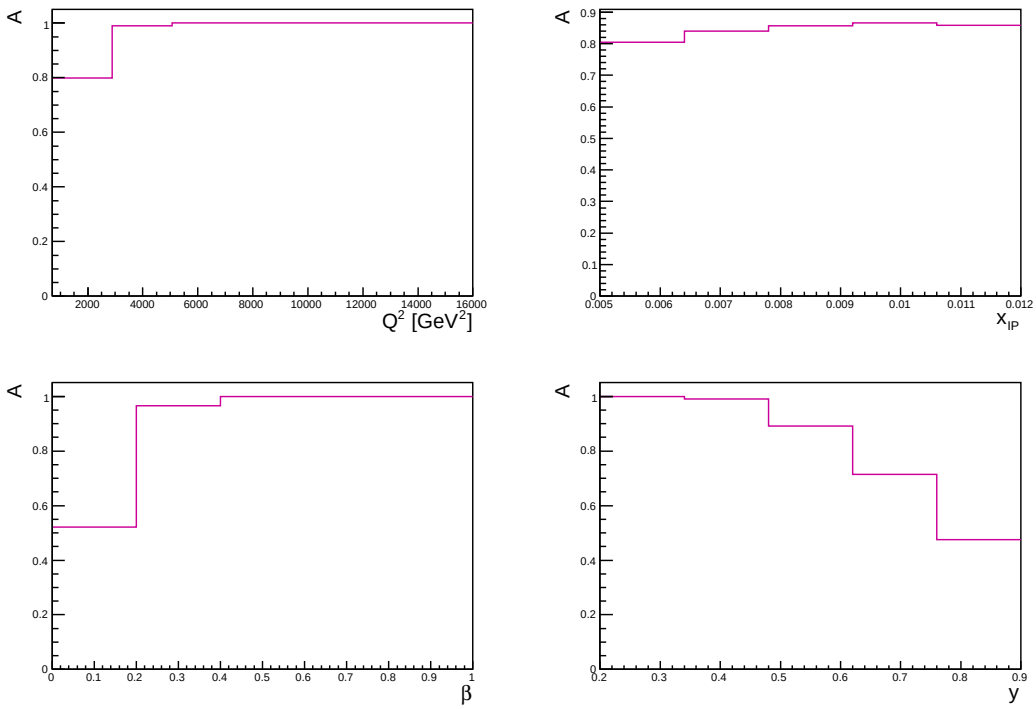

Fig. 7.7: The events selection efficiency A in the dependence on Q^2, x_{IP} β and y. $A \times 100$ is the percentage of events which can be measured by the detector. The kinematic region is given in (7.3).

7.2 Prediction for the LHeC CC cross section

For the Monte Carlo RAPGAP generated events in the kinematic region (7.3) in the LHeC experimental conditions the total cross section

$$\sigma^{LHeC}_{MC,DCC} = 923 \pm 1\,(\text{stat.})\,\text{fb} \tag{7.4}$$

was obtained.

The presumed relative statistical uncertainty of measurement assuming the LHeC conditions in (7.3) is $1/\sqrt{\text{luminosity} \times \text{acceptance} \times \text{cross section}}$.

The calculated total detector acceptance as the ratio of events cutted by (7.1) and (7.3) to events cutted only by (7.3) is 84.5%. Considering integrated luminosity $100\,\text{fb}^{-1}$ and the mentioned total acceptance, the number of detected events should be about 78000.

The diffractive charged current differential cross sections with the predicted statistical uncertainties in the dependence on Q^2, x_{IP}, β and y are shown in the Fig. 7.10. Events in the figure were selected by the (7.3) cuts. It was found that in the LHeC kinematic region the reggeon contribution is negligible (around 1% of the total cross section).

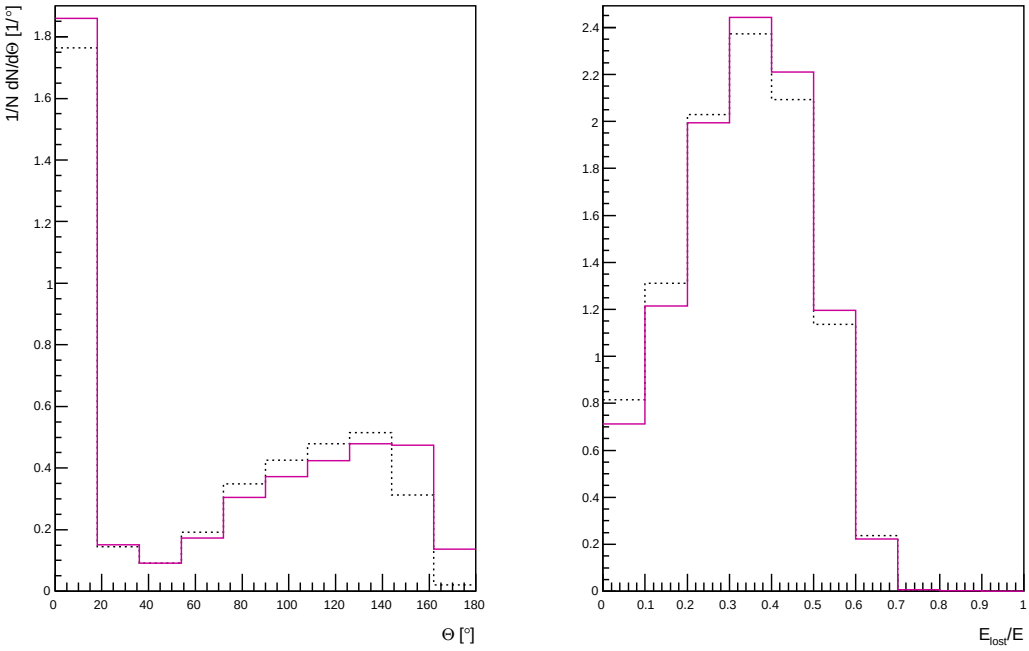

Fig. 7.8: **Left figure:** The differential distribution of number of hadrons per event going to the Θ angle. The histogram is normalized to the mean number of hadrons produced in event. **Right figure:** The histogram of the ratio of lost energy E_{lost} (caused by undetectable hadrons) to total event energy E. The histogram is normalized to 1. For both figures the pinkish solid lines are the histograms of events, which satisfy the (7.3) cuts, the dotted black lines are the histograms of events, which were cutted by both (7.3) and (7.1) cuts.

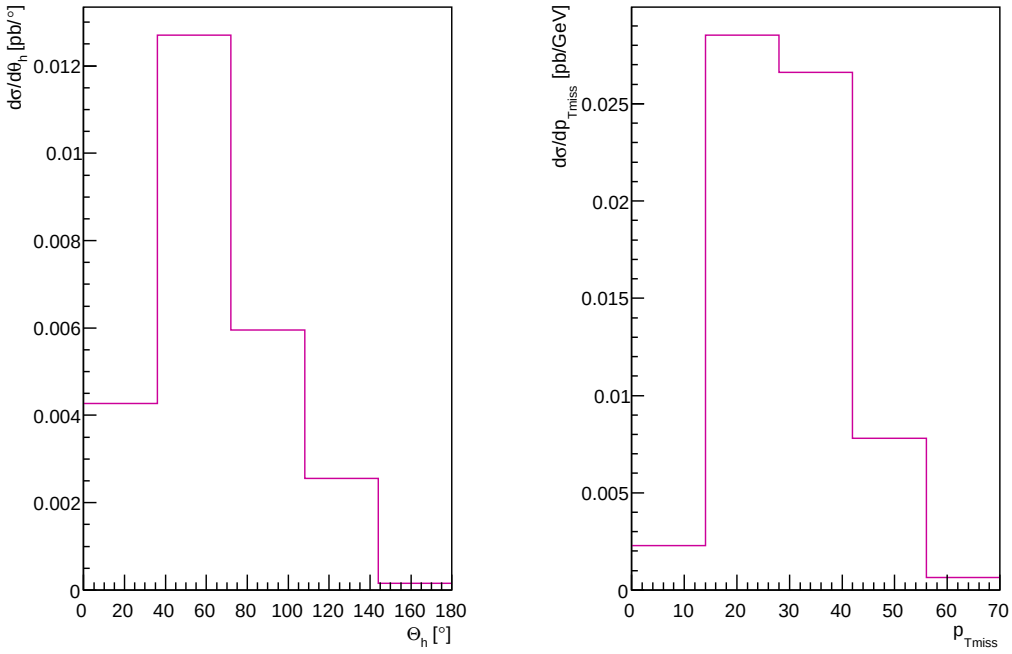

Fig. 7.9: The differential cross sections of the hadronic state angle Θ_h and transverse momentum p_{Tmiss}. The kinematic region is given in (7.3).

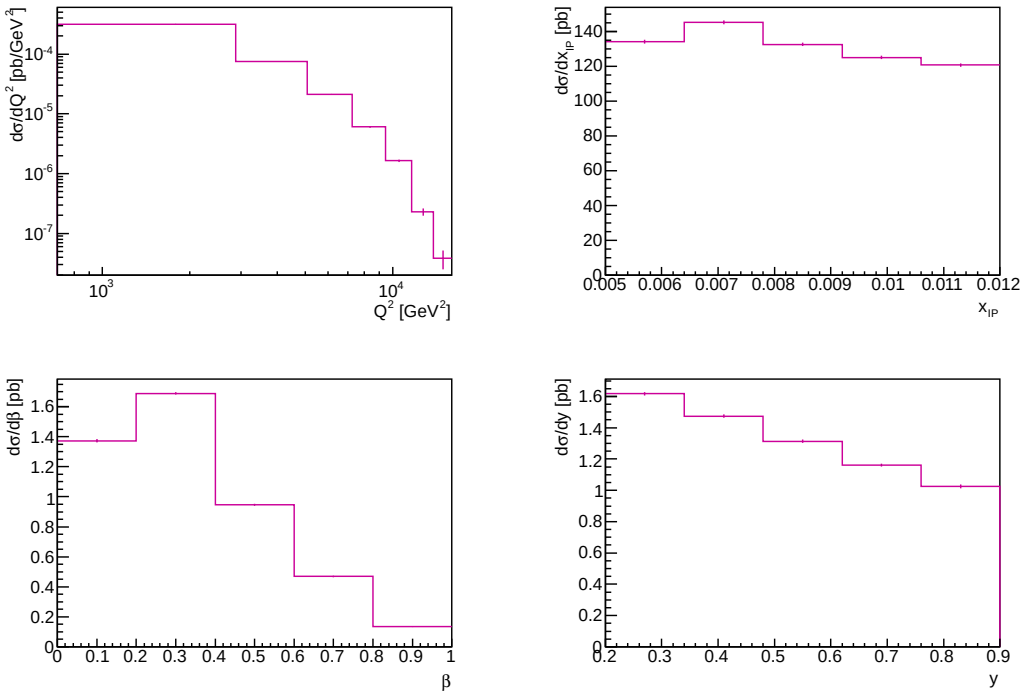

Fig. 7.10: The differential cross sections of Q^2, x_{IP}, β and y predicted for LHeC experimental layout. The plotted histograms errors are expected statistical uncertainties of measurement for integrated luminosity of $100\,\mathrm{fb}^{-1}$. The kinematic region is given in (7.3).

Chapter 8

Summary

The test of the MC RAPGAP simulation and the further analysis of diffractive charged current DIS was provided using the layout and the results of H1 experiment [6]. In spite of not knowing the exact parameters applied by H1 collaboration to the MC RAPGAP simulation, obtained MC distributions by myself and H1 collaboration are very similar.

In H1 configuration at integrated luminosity $61.6\,\mathrm{pb}^{-1}$ in the kinematic region $Q^2 > 200\,\mathrm{GeV}^2$, $y < 0.9$, $|t| < 1\,\mathrm{GeV}^2$ and $x_{IP} < 0.05$, 20 events were predicted by myself using MC RAPGAP. The real number of measured events is 10, it corresponds to the events selection efficiency around 50% in [6].

Then MC RAPGAP was used to predict the cross section of diffractive charged current DIS in the experimental conditions of the LHeC. The kinematics of generated events was studied and the suitable cuts were suggested.

The prediction for the LHeC, supposing the kinematic region (7.3), the integrated luminosity $100\,\mathrm{fb}^{-1}$ and the detector acceptance 84.5%, gives ~ 78000 events. This is obviously much more than in H1's case so such measurement enables to study properties of the diffractive charged current processes in a more detailed way. The prediction has to be specified, when the final detector setup will be known.

Bibliography

[1] J. Chyla, "Quarks, partons and Quantum Chromodynamics.".

[2] **H1 Collaboration** Collaboration, C. Adloff *et al.*, "Measurement and QCD analysis of neutral and charged current cross-sections at HERA," *Eur.Phys.J.* **C30** (2003) 1–32, arXiv:hep-ex/0304003 [hep-ex].

[3] B. Foster, "Deep inelastic scattering at HERA," *Int.J.Mod.Phys.* **A13** (1998) 1543–1622, arXiv:hep-ex/9712030 [hep-ex].

[4] H. Abramowicz, "Diffraction and the Pomeron," *Int.J.Mod.Phys.* **A15S1** (2000) 495–520, arXiv:hep-ph/0001054 [hep-ph].

[5] L. Gribov, E. Levin, and M. Ryskin, "Semihard Processes in QCD," *Phys.Rept.* **100** (1983) 1–150.

[6] **H1 Collaboration** Collaboration, A. Aktas *et al.*, "Measurement and QCD analysis of the diffractive deep-inelastic scattering cross-section at HERA," *Eur.Phys.J.* **C48** (2006) 715–748, arXiv:hep-ex/0606004 [hep-ex].

[7] *Diffraction in Charged Current*. 2004.

[8] **H1 Collaboration** Collaboration, T. Ahmed *et al.*, "Deep inelastic scattering events with a large rapidity gap at HERA," *Nucl.Phys.* **B429** (1994) 477–502.

[9] A. Hebecker, "Diffraction in deep inelastic scattering," *Phys.Rept.* **331** (2000) 1–115, arXiv:hep-ph/9905226 [hep-ph].

[10] David Šálek, "Dijet Production in Diffractive *ep* Interactions," diploma thesis, Charles University in Prague, 2006.

[11] **Gargamelle Neutrino Collaboration** Collaboration, F. Hasert *et al.*, "Observation of Neutrino Like Interactions Without Muon Or Electron in the Gargamelle Neutrino Experiment," *Phys.Lett.* **B46** (1973) 138–140.

[12] **H1 Collaboration** Collaboration, T. Ahmed *et al.*, "First measurement of the charged current cross-section at HERA," *Phys.Lett.* **B324** (1994) 241–248.

[13] S. L. Glashow, "Towards a unified theory - threads in a tapestry," December, 1979. http://www.nobelprize.org/nobel_prizes/physics/laureates/1979/. Nobel lecture.

[14] A. Salam, "Gauge unification of fundemantal forces," December, 1979. http://www.nobelprize.org/nobel_prizes/physics/laureates/1979/. Nobel lecture.

[15] S. Weinberg, "Conceptual foundations of the unified theory of weak and electromagnetic interactions," December, 1979. http://www.nobelprize.org/nobel_prizes/physics/laureates/1979/. Nobel lecture.

[16] C. Rubbia, "Experimental observation of the intermediate vector bosons W^+, W^- and Z^0," December, 1984. http://www.nobelprize.org/nobel_prizes/physics/laureates/1984/. Nobel lecture.

[17] N. Werner, *Measurement of the Charged Current Cross Section in Positron-Proton Collisions at HERA*. Dissertation, Universität Zürich, 2004.

[18] www-zeus.desy.de/physics/lumi/.

[19] "Super microscope HERA." DESY, 2002.

[20] M. Klein and R. Yoshida, "Collider Physics at HERA," *Prog.Part.Nucl.Phys.* **61** (2008) 343–393, arXiv:0805.3334 [hep-ex].

[21] **H1 Collaboration** Collaboration, I. Abt *et al.*, "The H1 detector at HERA,".

[22] J. Abelleira Fernandez, C. Adolphsen, P. Adzic, A. Akay, H. Aksakal, *et al.*, "A Large Hadron Electron Collider at CERN," arXiv:1211.4831 [hep-ex].

[23] "CERN LHC the guide," 2009. CERN-Brochure-2009-003-Eng.

[24] http://home.web.cern.ch/about/accelerators/large-hadron-collider.

[25] O. S. Bruning, P. Collier, P. Lebrun, S. Myers, R. Ostojic, *et al.*, "LHC Design Report. 1. The LHC Main Ring,".

[26] O. Buning, P. Collier, P. Lebrun, S. Myers, R. Ostojic, *et al.*, "LHC Design Report. 2. The LHC infrastructure and general services,".

[27] M. Benedikt, P. Collier, V. Mertens, J. Poole, and K. Schindl, "LHC Design Report. 3. The LHC injector chain,".

[28] **LHeC Study Group** Collaboration, J. Abelleira Fernandez *et al.*, "A Large Hadron Electron Collider at CERN: Report on the Physics and Design Concepts for Machine and Detector," *J.Phys.* **G39** (2012) 075001, arXiv:1206.2913 [physics.acc-ph].

[29] J. Dainton, M. Klein, P. Newman, E. Perez, and F. Willeke, "Deep inelastic electron-nucleon scattering at the LHC," *JINST* **1** (2006) P10001, arXiv:hep-ex/0603016 [hep-ex].

[30] B. Andersson, S. Mohanty, and F. Soderberg, "Recent developments in the Lund model," arXiv:hep-ph/0212122 [hep-ph].

[31] H. Jung, *The RAPGAP Monte Carlo for Deep Inelastic Scattering*, 2011.

[32] G. Ingelman and P. Schlein, "Jet Structure in High Mass Diffractive Scattering," *Phys.Lett.* **B152** (1985) 256.